Electric Power Systems Research 212 (2022) 108337

Contents lists available at ScienceDirect

Electric Power Systems Research

journal homepage: www.elsevier.com/locate/epsr

Impact of decentralized microgrids optimal energy management on power system dynamics

Juan S. Giraldo [a], Mohammed Ahsan Adib Murad [b,*], Taulant Kërçi [c], Federico Milano [d]

[a] Faculty of Electrical Engineering, Mathematics, and Computer Science, University of Twente, The Netherlands
[b] DIgSILENT GmbH, Germany
[c] EirGrid Group, Ireland
[d] School of Electrical & Electronic Engineering, University College Dublin, Ireland

ARTICLE INFO

Keywords:
Microgrids (MGs)
Power system dynamics
Renewable energy source (RES)
Energy storage system (ESS)
Frequency regulation
Optimal energy management (OEM)

ABSTRACT

This paper proposes a unified framework between the optimal energy management (OEM) problem of grid-connected microgrids and the frequency control of power systems through time-domain simulations. The proposed formulation is aimed at analyzing how different objectives for the microgrid OEM and control strategies affect the system frequency regulation. Each OEM model minimizes the microgrid local objective while ensuring energy reserves and operational limits by solving a two-stage stochastic optimization mathematical model. Two control approaches of microgrids are considered, namely, *greedy* and *cooperative*. The proposed framework is evaluated considering the IEEE 39-bus test system, including multiple microgrids with different energy storage capacities, and control strategies. Results show an improvement in system's frequency deviation when MGs operate in the cooperative configuration while simultaneously reducing their operational costs.

1. Introduction

1.1. Motivation

The optimal energy management (OEM) of a microgrid (MG) consists in finding the most advantageous operational set-points for dispatchable units to achieve selected objectives guaranteeing operational constraints. From the MG perspective, these objectives generally include the minimization of the operating costs, power losses, imported energy, gas emissions, among others [1].

At the same time, as the interaction between transmission system operators (TSOs) and MGs at the distribution level increases, it is expected that their cooperation assists to improve congestion problems at the point of common coupling (PCC), relieving transmission lines overloading, providing voltage control and frequency regulation support, among others [2]. Moreover, the insertion of energy sources with very limited to no rotational inertia, such as solar PV or wind turbines, add an additional layer of technical challenges to maintain the stability of the system [3] and frequency stability is one of the main concern [4].

Hence, considering the potential impacts of MGs on the transmission system and analyzing the effect that different OEM configurations might have on power system dynamics is of great interest for future power systems. This paper focuses specifically on discussing such an impact through aggregated modeling and simulation of microgrids, their OEM and the power grid.

1.2. Literature review

The interaction between TSOs and distribution system operators to increase penetration of intermittent renewable energy sources (RESs) has drawn considerable attention in the last few years, from economic aspects like market architectures and business models [5], through operational coordination models and solution techniques [6], to game-theoretical mechanisms for flexibility aggregators [7]. However, the insertion of RES usually come with a reduction of the rotational inertia, which may lead to unintentional load/generation shedding or even to a system blackout [8].

An option to help increase RES penetration is the inclusion of battery energy storage systems (BESS) technologies acting in the primary frequency control [9]. Numerous research works have been done in this direction, as in [10], where the authors proposed a method to define the sizing and control of BESS to contribute in the primary frequency control. In [11], the authors introduced a distributed control of BESS to improve frequency regulation, and in [12], a comprehensive review of fast-responding energy storage technologies is presented,

* Corresponding author.
E-mail address: mohammed.murad@ucdconnect.ie (M.A.A. Murad).

https://doi.org/10.1016/j.epsr.2022.108337
Received 9 October 2021; Received in revised form 7 March 2022; Accepted 2 July 2022
Available online 25 July 2022

including gaps, limitations, and recommendations for future research in frequency regulation.

Virtual power plants (VPPs) are another solution to address the RES penetration problem. This can be seen in [13], where VPPs are considered as participants of day-ahead energy and spinning reserve markets, or in [14], where the impact of VPPs in short-term transient response has been studied, showing that a coordinated control between BESS and distributed energy resources enhances the frequency response when compared to uncoordinated instances.

MGs have also be considered as an alternative for the provision of ancillary services to TSOs allowing the integration of RES. Previous work has analyzed the impact of MGs on power system dynamics, as in [15], where energy reserves from multiple MGs are used for frequency regulation implementing a coordinated centralized control. Similarly, in [16], the authors examined the effects of greedy MGs on the power system frequency regulation through time-domain simulations (TDS). However, the OEM of the MGs is simplified using an event-driven heuristic representation. On the other hand, it is common in OEM formulations to overlook the MG dynamic behavior and their interaction with the upstream power grid.

For instance, the optimal control of power flows between MGs and the main grid has been studied in [17], showing the advantages and benefits of applying coordinated control within a system of MGs or in [18], where the OEM of grid-connected unbalanced MGs has been studied. Another alternative is to consider operating flexibility regions as proposed in [19] for distribution networks, or calculating energy reserves as in [20]; however, the effect of these approaches in the power system dynamic behavior has not yet been tested.

1.3. Contributions

This paper proposes a unified framework between the OEM problem of grid-connected MGs and the frequency control of power systems through TDS. The proposed formulation allows analyzing how the objective function of the OEM and the control strategies of the MGs affect the system frequency regulation. With this aim, an aggregated MG dynamic model is introduced with the assumption that MG internal time constants are small against the ones of the high voltage transmission system.

Similarly to [20], the OEM model minimizes the MG main objective while ensuring energy reserves and operational limits. However, in the proposed formulation, the MG energy reserves and the power at the PCC are calculated using decentralized formulations solving two-stage stochastic optimization mathematical models with two different objectives:

- Minimizing local operational cost (*greedy*),
- Maximizing energy reserves (*cooperative*).

Uncertainties within each MG come from local loads and renewable energy sources, and errors related to the operation are modeled using a traditional rolling horizon approach. The assessment of the proposed unified framework is based on the IEEE 39-bus test system, modified to include multiple MGs, a multi-objective OEM, and two control strategies to implement the OEM planning dispatch.

1.4. Organization

The remainder of the paper is organized as follows. Section 2 presents the OEM model of MGs (Section 2.1), MG aggregated model and control (Section 2.2), the system dynamic model (Section 2.3), and the approach followed to perform the simulations based on a rolling horizon for the OEM (Section 2.4). Section 3 discusses the case study based on the IEEE 39-bus system. Finally, Section 4 draws relevant conclusions.

2. Proposed microgrid models

2.1. Microgrid optimal energy management

The stochastic optimization model introduced in this paper has been adapted from [21] to consider multiple periods, ESS, and energy reserves. Let $s \in \Omega_S$, as one scenario in a finite set of scenarios, where the vector of uncertain parameters, conformed by the load, solar irradiance, and wind speed, is represented by $\boldsymbol{\eta}_s$. Similarly, the set of dispatchable energy sources, including the connection at the PCC can be represented as Ω_D, and the set of time periods as Ω_T. Overall, each microgrid is assumed to be composed by dispatchable energy sources (e.g., BESS, synchronous generators), non-dispatchable sources (e.g., solar PV, wind turbines), and conventional loads. Thus, the vector of first-stage variables (*here-and-now*) $\boldsymbol{\xi}_I = \{p_{g,t}, p_{d,t}, \forall t \in \Omega_T, d \in \Omega_D\}$ represents the exchange of active power between the microgrid and the main grid and the set point of dispatchable units at each time period; while the vector of second-stage variables (*wait-and-see*), $\boldsymbol{\xi}_{II}(\boldsymbol{\eta}_s) = \{\xi_{s,t}, \forall t \in \Omega_T, s \in \Omega_S\}$, embodies voltages, currents, state of charge (SOC) from BESS, and deviations from set-points at each time period in each scenario. Consider $a_{d,t}$ as the generation costs of each dispatchable energy source (d) inside the microgrid and b_t as the energy cost of importing power from the main grid. Hence, the total energy cost of the microgrid is expressed as

$$\phi(\boldsymbol{\xi}_I) = \sum_{t\in\Omega_T}\sum_{d\in\Omega_D} a_{d,t}\, p_{d,t} + \sum_{t\in\Omega_T} b_t\, p_{g,t}\,. \tag{1}$$

The energy reserves can be expressed as a *deadband* with a maximum and minimum SOC. In this paper, the deadband is calculated as

$$\mu_t^{soc} = \sum_{s\in\Omega_S} \mathbb{P}_s \mathrm{SOC}_{t,s}, \quad \forall t \in \Omega_T \tag{2a}$$

$$\left(\sigma_t^{soc}\right)^2 = \sum_{s\in\Omega_S} \mathbb{P}_s \left(\mathrm{SOC}_{t,s}\right)^2 - \left(\mu_t^{soc}\right)^2, \quad \forall t \in \Omega_T \tag{2b}$$

$$s_c^{max}{}_t = \mu_t^{soc} + \psi\, \sigma_t^{soc};\ s_c^{min}{}_t = \mu_t^{soc} - \psi\, \sigma_t^{soc},\ \forall t \in \Omega_T \tag{2c}$$

$$\mathcal{R}_t = s_c^{max}{}_t - s_c^{min}{}_t,\ \forall t \in \Omega_T \tag{2d}$$

where $\mathbb{P}_s$ stands for the probability or weighting factor of scenario s, μ_t^{soc} represents the average of the SOC, σ_t^{soc} the standard deviation, and ψ a parameter (defined by the microgrid operator) to control the energy reserves.

Furthermore, the average cost of deviating from the set-point $\boldsymbol{\xi}_I^*$ is penalized by c_t and λ_t is considered as the imbalance price for the TSO for the expected use of the energy reserves. These costs can be expressed as,

$$\chi(\boldsymbol{\xi}) = \sum_{t\in\Omega_T}\sum_{s\in\Omega_S} \mathbb{P}_s \sum_{d\in\Omega_D} c_t |\mathcal{P}_{d,t,s}| - \lambda_t \mathcal{R}_t\,, \tag{3}$$

where $\boldsymbol{\xi} = [\boldsymbol{\xi}_I, \boldsymbol{\xi}_{II}(\boldsymbol{\eta}_s)]$. Finally, the deterministic equivalent can be written as

$$\begin{aligned} \min.\quad & \mathrm{OF}(\boldsymbol{\xi}) = \gamma\, \phi(\boldsymbol{\xi}_I) + \tau\, \chi(\boldsymbol{\xi}) \\ \text{s.t.}\quad & \boldsymbol{k}(\boldsymbol{\xi}_I) \le 0\,, \\ & \boldsymbol{h}(\boldsymbol{\xi}) \le 0\,, \qquad \forall s \in \Omega_S\,, \end{aligned} \tag{4}$$

where $\boldsymbol{k}(\boldsymbol{\xi}_I)$ represents the constraints dependent on the first-stage variables only, e.g., unit operational limits, and $\boldsymbol{h}(\boldsymbol{\xi})$ the constraints dependent on both stage variables, e.g., power flow constraints and system operational constraints. Furthermore, it can be seen that the deterministic equivalent is a bi-objective mathematical model so the microgrid operator can define its priorities, i.e., fully greedy ($\gamma = 1$ and $\tau = 0$) or fully cooperative ($\gamma = 0$ and $\tau = 1$). Notice that the TSO can incentivize the MGs to provide more energy reserves and participate to the frequency regulation control by modifying parameter λ_m, e.g., using locational marginal pricing (LMP) or any other mechanism. Moreover, the set of scenarios can be determined with any scenario generation technique, e.g., conditional moment matching, Markov chains, Monte Carlo methods, etc. In this paper, the $2m+1$ point estimate method has been used to generate the data trajectories as in [21].

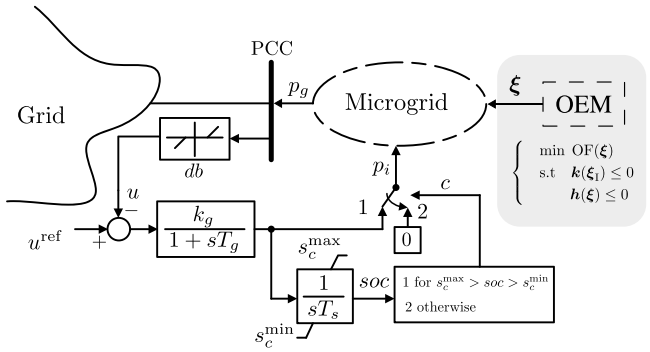

Fig. 1. A microgrid connected to the transmission system considering its OEM and dynamic control model.

2.2. Microgrid dynamic control

This section describes the proposed dynamic model of the MG with two different mode of operation, namely, cooperative and greedy control approach. Fig. 1 illustrates a MG connected to the transmission grid, where the exchange of active power between the microgrid and transmission system is p_g.

2.2.1. Cooperative MG control

In cooperative mode, the microgrid uses the energy reserves to participate to the frequency control. Therefore the measured signal is the frequency at the PCC, where the reference is defined as $u^{\text{ref}} = \omega^{\text{ref}} = 1$ pu ($u = \omega_{\text{pcc}}$) and the frequency deadband set to $db = 0.001$ pu. The controller output p_i in Fig. 1 is given by

$$\frac{d}{dt}p_i = \frac{1}{T_g}(k_g(u^{\text{ref}} - u) - p_i)\,, \tag{5}$$

where k_g and T_g are the controller gain and time constant, respectively.

During frequency control, the available energy capacity of the MG is limited by the SOC. Therefore, another controller tracks the SOC based on the real time active power (p_i) utilized by the controller. The SOC is obtained by an anti-windup integrator limited by the maximum and minimum SOC. Mathematically,

$$\begin{aligned}
&\text{if SOC} \ge s_c^{\max} \text{ and } \frac{d}{dt}\text{SOC} \ge 0:\\
&\quad \text{SOC} = s_c^{\max} \text{ and } \frac{d}{dt}\text{SOC} = 0\,,\\
&\text{if SOC} \le s_c^{\min} \text{ and } \frac{d}{dt}\text{SOC} \le 0:\\
&\quad \text{SOC} = s_c^{\min} \text{ and } \frac{d}{dt}\text{SOC} = 0\,,\\
&\text{otherwise}:\\
&\quad \frac{d}{dt}\text{SOC} = \frac{p_i}{T_s}\,,
\end{aligned} \tag{6}$$

where $T_s = \frac{1}{\alpha \text{EC}}$ is the charging/discharging time constant; and EC is the BESS energy capacity and α the charging/discharging rate. Note that $s_c^{\min}$ and $s_c^{\max}$ are obtained from the OEM.

2.2.2. Greedy MG control

The exchange of active power (p_g) between the MG and the transmission grid are held fixed from the value obtained in the OEM. In such a control scheme, the microgrid prioritizes its own operation and does not contribute to the frequency control.

2.3. Stochastic long-term power system model

This paper considers a long-term dynamic power system model represented by a set of hybrid non-linear stochastic differential–algebraic equations [22], as follows:

$$\begin{aligned}
&\frac{d}{dt}\boldsymbol{x} = \boldsymbol{f}(\boldsymbol{x}, \boldsymbol{y}, \boldsymbol{u}, \boldsymbol{z}, \frac{d}{dt}\boldsymbol{\eta})\,,\\
&\boldsymbol{0} = \boldsymbol{g}(\boldsymbol{x}, \boldsymbol{y}, \boldsymbol{u}, \boldsymbol{z}, \boldsymbol{\eta})\,,\\
&\frac{d}{dt}\boldsymbol{\eta} = \boldsymbol{a}(\boldsymbol{x}, \boldsymbol{y}, \boldsymbol{\eta}) + \boldsymbol{b}(\boldsymbol{x}, \boldsymbol{y}, \boldsymbol{\eta})\,\boldsymbol{\zeta}\,,
\end{aligned} \tag{7}$$

where $\boldsymbol{f}$ and $\boldsymbol{g}$ represent the differential and algebraic equations, respectively; $\boldsymbol{x}$ and $\boldsymbol{y}$ represent the state and algebraic variables, such as generator rotor speeds and bus voltage angles, respectively; $\boldsymbol{u}$ represents the inputs, such as the schedules of synchronous generators; $\boldsymbol{z}$ represents discrete variables; $\boldsymbol{\eta}$ represents the stochastic characterization of wind speed; $\boldsymbol{a}$ and $\boldsymbol{b}$ are the *drift* and *diffusion* of the SDEs, respectively; and $\boldsymbol{\zeta}$ is the white noise.

Eq. (7) includes the dynamic models of conventional machines (4th order models) and their primary controllers; automatic generation control; wind power plants (5th order Doubly-Fed Induction Generator) [23]; and the model of MGs.

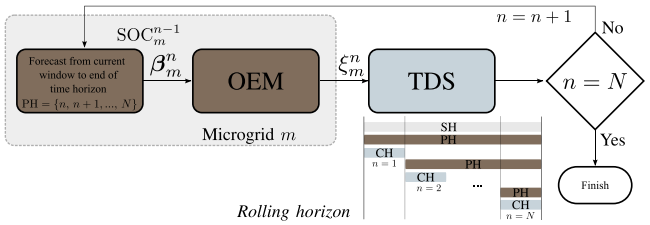

Fig. 2. Flowchart of the testing methodology considering a rolling horizon framework.

2.4. Rolling horizon and simulation approach

A rolling horizon framework is considered in this paper to cope with changes in the system, i.e., generation set-points, tap positions, topological changes, updated forecast data, etc. Three main components are considered: a scheduling horizon (SH), a prediction horizon (PH), and a control horizon (CH). The SH represents the total time span to be analyzed, discretized in equal time windows defined as SH $= \{1, 2, \ldots, N\}$. In the PH, random variables are assumed to be parameterized by known distribution functions and the OEM described in Section 2.1 is executed. The length of the PH is dynamic, and changes depending on the time window n, as PH $= \{n, n+1, \ldots, N\}$. Finally, in the CH, the decisions found in the PH are applied, and the dynamic response is assessed using TDS during the time window n.

The interaction between the OEM and the dynamic control of a MG m is performed hierarchically at each time window n. First, the OEM of a microgrid m receives a set of input parameters ($\boldsymbol{\beta}_m^n = \{p_m^f, \lambda_m, \text{SOC}_m^{n-1}\}$), containing the forecasted power from local RES and loads for the current prediction horizon, the forecasted price for energy reserves, and the most recent SOC from the TDS (assumed as known for $n = 1$). The OEM is solved to obtain the input parameters for the dynamic control, including the power set-point, the SOC of the BESS, the energy reserves, and the control approach. This information is embodied by $\boldsymbol{\xi}_m^n = \{p_g, \text{SOC}, s_{c\_n}^{\min}, s_{c\_n}^{\max}, c\}$ and communicated to the dynamic control. Once all dynamic controls are updated, a TDS simulation is performed for the duration of the time window n, considering the transmission system behavior, similar to [24]. This process is repeated until the last control horizon has been considered, as depicted in Fig. 2.

Finally, from the OF in (4), it can be seen that the total cost of the MGs depends on two terms: a day-ahead cost and an operation cost. The instantaneous operation cost of each MG is then calculated as

$$C_t = \mathrm{b}_t p_{g,t}^* - \lambda_t |p_{g,t}| + \sum_{d \in \Omega_{\mathrm{D}}} \mathrm{a}_{d,t} p_{d,t}^* + \mathrm{c}_t |p_{d,t}| \quad \forall\, t \in \Omega_{\mathrm{T}} \tag{8}$$

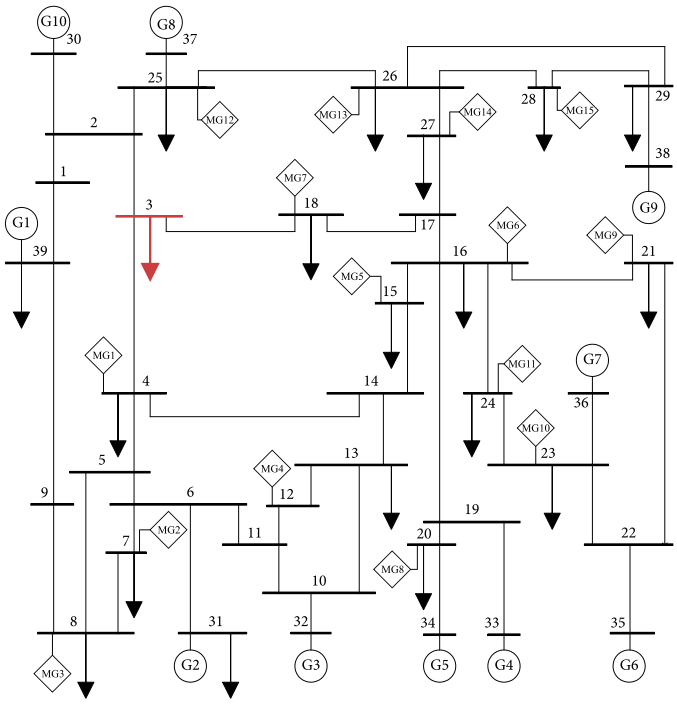

Fig. 3. IEEE 39-bus system with 15 microgrids.

where the first term represents the payment from the MG to the TSO due to the set-point from the OEM; the second term stands for the payment from the TSO to the MG for participating in the frequency control; the third one accounts for the cost of the set-point of the internal energy sources, and finally, the fourth term represents the cost of modifying the operation set-point of the internal energy sources.

3. Case study

The case study is based on the well-known IEEE New England 39-bus 10-machine system. Dynamic data of this system is available in [25]. The system includes 10 synchronous machines, 19 loads, 34 transmission lines and 12 transformers and the frequency of the system is 60 Hz. All synchronous generators are equipped with automatic voltage regulators, power system stabilizers and turbine governors (TGs). The TGs are coordinated through an automatic generation control.

Fifteen MGs with different capacities are connected at different load buses, namely, bus 4, 7, 8, 12, 15, 16, 18, 20, 21 and 23–28, as shown in Fig. 3. The total accumulated capacity of the MGs is 45 MW and the total nominal load is around 6 GW; hence, the total contribution of the MGs in the system is around 1%. The parameters of the cooperative frequency controller of all MGs are considered to be equal, namely $k_g = 15$, $T_g = 0.1$. While the constant for the SOC controller of all MGs is based on individual MG capacities. Finally, the MG stochastic optimization model is implemented in the Python language and solved using the Gurobi solver, while the TDS is solved using the Python-based software tool Dome [26].

3.1. Deterministic analysis

The deterministic case assumes perfect knowledge of the exogenous parameters in the system during the SH, e.g., RES, loads, etc. In this test case, two scenarios are analyzed: *conventional* and *low-inertia*. The difference between these scenarios is the number of conventional generators, being the low-inertia scenario the one with reduced total rotational inertia. Three different MG configurations are studied in each scenario, namely, no MGs, greedy MGs, and cooperative MGs. No

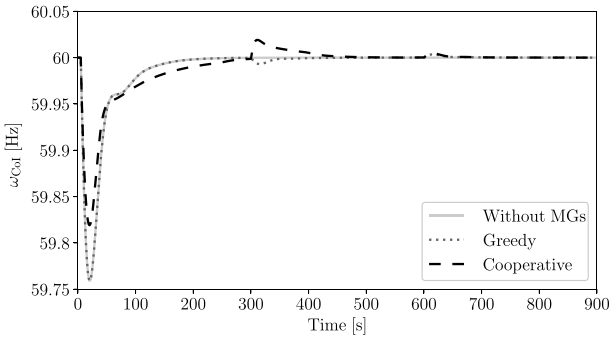

Fig. 4. Frequency response of the conventional scenario.

stochastic variations of the loads and generation are considered in this section (see Section 3.2 for a stochastic analysis).

3.1.1. Conventional scenario

This case study considers the original 39-bus system with the connected MGs. The test system is simulated for an SH of 15 min with a contingency happening at $t = 5$ s consisting of a 25% instantaneous load increase at bus 3 from its nominal value. The CH is defined as 5 min; hence, the OEM is executed three times in total. The frequency response of the center of inertia (CoI) is shown in Fig. 4, where the frequency excursion right after the contingency drops around 59.76 Hz if no MGs are considered. Note that Fig. 4 shows the most relevant part of the trajectories i.e., primary and secondary frequency response.

An almost identical result is obtained for all MGs operating under the greedy control; this is expected, since the greedy control uses the MG internal energy reserves to maintain the power at the PCC close to the set-point given by the OEM and does not participate to the frequency control. However, small differences are evidenced when the set-point changes due to the OEM, as in $t = 300$ s and in $t = 600$ s. On the other hand, when the MGs operate with the cooperative configuration, observe that the maximum frequency excursion is around 59.83 Hz. This is an improvement of around 70 mHz over the other two configurations. Notice that even with a small participation of MGs (1% of total load), the cooperative operation of the MGs would help to maintain the frequency within acceptable frequency boundaries.

3.1.2. Low-inertia scenario

This test case considers replacing approximately 25% of the system conventional generation capacity (three synchronous machines) with wind farms in buses 30–32. This share of wind energy is expected in future electricity grids, considering the current trends and goals. The SH, CH, and contingency have been defined as in the previous test case. The results in Fig. 5 show that the reduction of rotational inertia in the system increases the frequency excursion after the contingency compared to the conventional scenario discussed in the previous section. In this case, the frequency drops lower than 59.68 Hz when no MGs are considered and with the greedy control configuration. Whereas for the conventional scenario, the minimum frequency reached with the cooperative control is around 59.76 Hz, which corresponds to 80 mHz of improvement.

3.1.3. Microgrids' operation cost

It is assumed that $b_t = 53$ €/MWh remains constant since the CH is short (less than one hour). Also, $a_{d,t}$ is assumed to be known since it depends on each MG's local energy resources. Finally, the imbalance prices are assumed as constant within 15 min; then, $\lambda_t = 150$ €/MWh : $t < 900$ s and $\lambda_t = 180$ €/MWh : $t \geq 900$ s. The MG cost of the low-inertia scenario is calculated for the greedy (dashed line) and cooperative (continuous line) configurations, as depicted in Fig. 6 for MG1 connected at bus 4. It can be seen that the MG's instantaneous

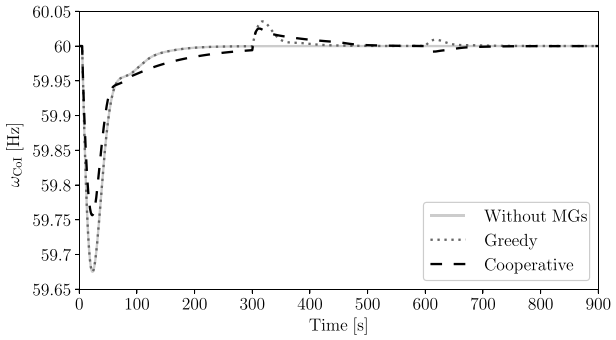

Fig. 5. Frequency response in low-inertia scenario.

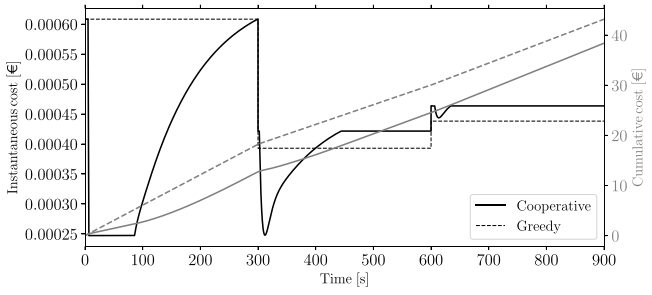

Fig. 6. Operation cost in low-inertia scenario — MG1.

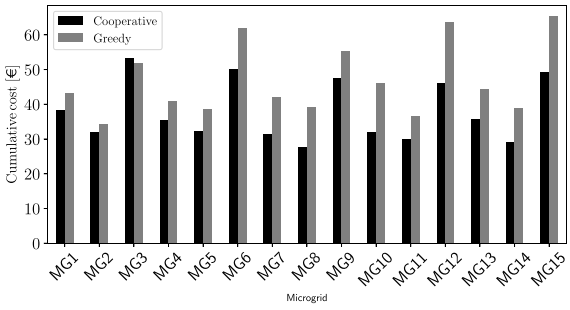

Fig. 7. Cumulative operation cost of MGs in low-inertia scenario.

cost decreases with its participation in the frequency control up to the MG's power limit, and increases gradually as the injected power returns to the set-point. The same behavior happens at each set-point change, i.e., at $t = 300$ s and $t = 600$ s. It can also be seen that the MG's cumulative cost decreases at the end of the SH from €43.2 to €38.4 (11%). In fact, the average cost reduction among all MGs is 18.5% with a maximum of 30.7% at MG10 and a minimum of −2.7% at MG3, as can be seen in Fig. 7, where the cumulative costs for all MGs are shown. These results indicate that the participation of MGs in the frequency control could be beneficial for both parties, but MG operators should carefully evaluate the benefit of their energy reserves. In fact, it is more costly for MG3 to participate to the frequency control than to be greedy.

3.2. Stochastic analysis

In this test case, a SH of 30 min is considered while keeping the CH to 5 min. The low-inertia scenario is considered. Uncertainty is included both in the PH and the CH steps of the rolling horizon framework. Hence, the objective of this test case is to assess the effect of the different control strategies considering the stochastic variations. Three scenarios are taken into account: without MGs, greedy control and cooperative control.

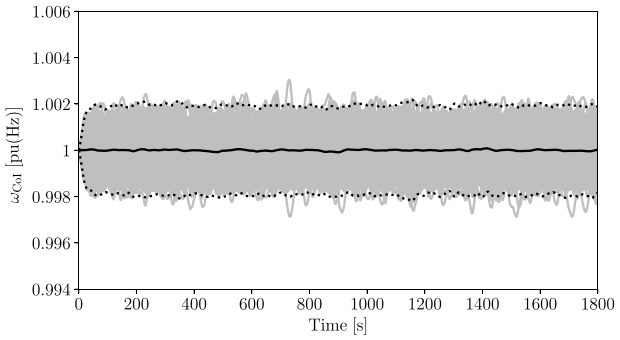

Fig. 8. Frequency of the CoI for the case without MGs. The gray lines represent each realization, the black thick line represents the average of the process, while the dotted line represents the average ±3 times the standard deviation.

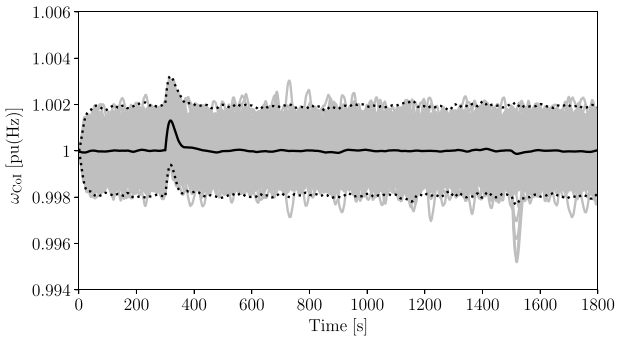

Fig. 9. Frequency of the CoI for the greedy approach. The gray lines represent each realization, the black thick line represents the average of the process, while the dotted line represents the average ±3 times the standard deviation.

3.2.1. Without MGs

This scenario does not consider any MGs in the system. The frequency of the CoI is shown in Fig. 8 where the gray lines represent each realization, the continuous black thick line represents the average of the process (mean value), while the dotted line represents the average ±3 times the standard deviation. A maximum standard deviation of 0.04365 Hz is obtained in this scenario. This scenario is utilized as a base case to compare the results obtained with other scenarios.

3.2.2. Greedy MGs

In this scenario, all MGs are considered to be operating in the greedy mode. The frequency of the CoI is shown in Fig. 9. Notice that significant changes in the MGs set-points are relevant to the system frequency, as can be seen in Fig. 10, particularly in the time windows ($300 \leq t \leq 600$ s) and ($1200 \leq t \leq 1500$ s), where the set-points of three different trajectories are displayed for the MG connected at bus 4. The changes in the MGs set-point, in fact, make the dynamic behavior of the greedy approach (Fig. 9) slightly worse than the case without MGs (Fig. 8) as can be estimated by comparing the standard deviation in this scenario (0.04395 Hz).

3.2.3. Cooperative MGs

This scenario assumes all MGs to be operating in the cooperative configuration. Fig. 11 shows that the deviation of the frequency of the CoI during the SH is considerably lower in the cooperative case than in the greedy one. In this configuration, the obtained standard deviation is 0.02818 Hz, which means an improvement of around 35% compared to the case with no MGs. Fig. 12 shows three trajectories of p_g for the MG connected at bus 4. It is relevant to note that the power of the MG deviates from the set-point imposed by the OEM depending on the system requirements to provide frequency support.

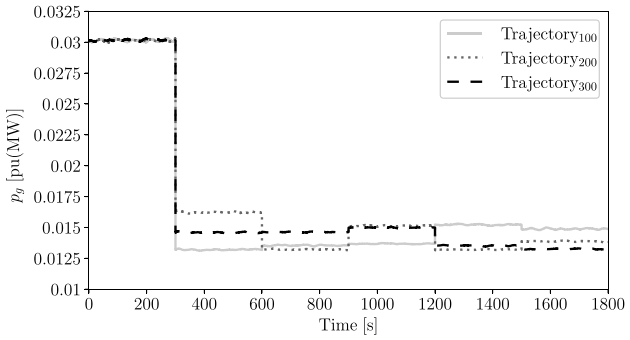

Fig. 10. Active power of MG connected at bus 4 for greedy approach.

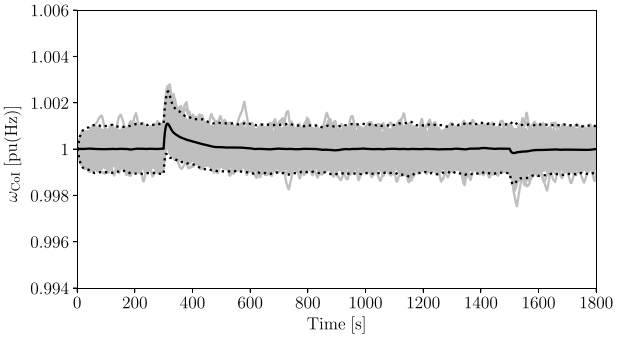

Fig. 11. Frequency of the CoI for the cooperative approach. The gray lines represent each realization, the black thick line represents the average of the process, while the dotted line represents the average ±3 times the standard deviation.

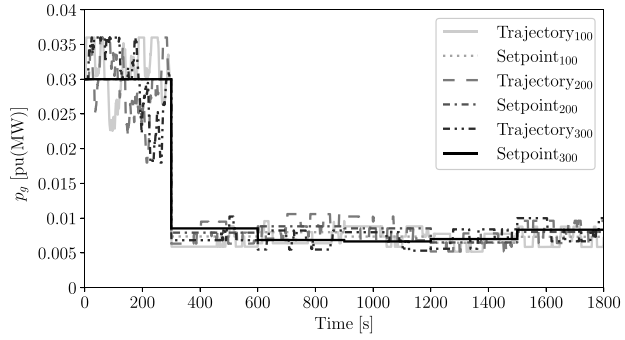

Fig. 12. Active power of MG connected at bus 4 for cooperative approach.

3.2.4. Microgrids' operation cost

The impact of the MGs participating in the frequency control regarding their operation cost is also assessed. The cost parameters in Section 3.1.3 are used for this regard, considering the stochastic trajectories for the cooperative approach. Results are shown for MG8 located at bus 20 in Fig. 13 for three imbalance costs, namely, λ_t = [145, 150, 155] €/MWh. It can be seen that the MG's operational cost is affected positively with the value of λ, which might be a motivator for MGs to participate to the frequency control. For instance, MG8 perceives a reduction in its operating cost of around 36%, reducing from an average of €56.4 in the greedy scenario to around €35.5 when $\lambda_t = 145$ €/MWh.

4. Conclusions

This paper proposes an unified framework to study the impact of the OEM and the frequency control of MGs on the dynamic response of

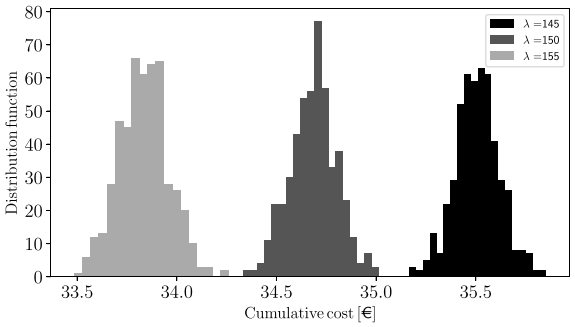

Fig. 13. Histogram of operation cost for different imbalance prices — MG8.

power systems. A two-stage stochastic programming problem is used to obtain the optimal MG set-points and energy reserves using a rolling horizon framework. Two control approaches are tested, namely, greedy and cooperative. Finally, an aggregated dynamic model is introduced to cope with the MGs interaction in the frequency control.

Results show that the MGs operating in the cooperative mode are able to provide frequency support considering small perturbations in different scheduling horizons and under uncertainty. When tested in the low-inertia scenario with reduced conventional generation (25% of generating capacity from wind), it is found that MGs operated with the cooperative mode are able to support in the primary frequency control to maintain safe boundaries, without significantly compromising the optimal scheduling determined with their OEM. Another interesting result of the stochastic analysis is that the dynamic performance of power systems with MGs operating in the greedy approach is slightly worse than systems without MGs. This result indicates the importance of cooperation of MGs in future power systems. It is also relevant to observe that the cooperative operation of MGs can be motivated by TSOs using LMP or any other pricing mechanism, and note that an appropriate selection of the energy reserves from MGs is highly important to reduce their operation cost. Future work will analyze the impact of different contingencies and the use of voltage–frequency control alternatives for improving power system stability using RES [27].

CRediT authorship contribution statement

Juan S. Giraldo: Conceptualization, Methodology, Software, Validation, Writing – original draft. **Mohammed Ahsan Adib Murad:** Conceptualization, Methodology, Software, Validation, Writing – original draft. **Taulant Kërçi:** Conceptualization, Methodology, Software, Validation, Writing – original draft. **Federico Milano:** Validation, Writing – review & editing.

Declaration of competing interest

The authors declare that they have no known competing financial interests or personal relationships that could have appeared to influence the work reported in this paper.

Acknowledgments

J. S. Giraldo was financially supported by the Netherlands Enterprise Agency (RVO) – DEI+ project 120037 "*Het Indiëterrein: Een slimme buurtbatterij in de oude weverij*".

F. Milano was supported by Sustainable Energy Authority of Ireland (SEAI), under the project FRESLIPS, Grant No. RDD/00681.

References

[1] F. Katiraei, R. Iravani, N. Hatziargyriou, A. Dimeas, Microgrids management, IEEE Power Energy Magaz. 6 (3) (2008) 54–65.

[2] T. Krechel, F. Sanchez, F. Gonzalez-Longatt, H. Chamorro, J.L. Rueda, Transmission system-friendly microgrids: an option to provide ancillary services, in: Distributed Energy Resources in Microgrids, Elsevier, 2019, pp. 291–321.

[3] L. Mehigan, D. Al Kez, S. Collins, A. Foley, B. Ó'Gallachóir, P. Deane, Renewables in the European power system and the impact on system rotational inertia, Energy 203 (2020) 117776.

[4] F. Milano, F. Dörfler, G. Hug, D.J. Hill, G. Verbič, Foundations and challenges of low-inertia systems (invited paper), in: 2018 Power Systems Computation Conference (PSCC), 2018, pp. 1–25, http://dx.doi.org/10.23919/PSCC.2018.8450880.

[5] M. Barbero, C. Corchero, L.C. Casals, L. Igualada, F.-J. Heredia, Critical evaluation of European balancing markets to enable the participation of demand aggregators, Appl. Energy 264 (2020) 114707.

[6] A.G. Givisiez, K. Petrou, L.F. Ochoa, A review on TSO-dso coordination models and solution techniques, Electr. Power Syst. Res. 189 (2020) 106659.

[7] G. Tsaousoglou, J.S. Giraldo, P. Pinson, N.G. Paterakis, Mechanism design for fair and efficient DSO flexibility markets, IEEE Trans. Smart Grid 12 (3) (2021) 2249–2260.

[8] P. Tielens, D. Van Hertem, The relevance of inertia in power systems, Renew. Sustain. Energy Rev. 55 (2016) 999–1009.

[9] K. Divya, J. Østergaard, Battery energy storage technology for power systems—An overview, Electr. Power Syst. Res. 79 (4) (2009) 511–520.

[10] A. Oudalov, D. Chartouni, C. Ohler, Optimizing a battery energy storage system for primary frequency control, IEEE Trans. Power Syst. 22 (3) (2007) 1259–1266.

[11] T. Zhao, A. Parisio, J.V. Milanović, Distributed control of battery energy storage systems for improved frequency regulation, IEEE Trans. Power Syst. 35 (5) (2020) 3729–3738.

[12] U. Akram, M. Nadarajah, R. Shah, F. Milano, A review on rapid responsive energy storage technologies for frequency regulation in modern power systems, Renew. Sustain. Energy Rev. 120 (2020) 109626.

[13] E. Mashhour, S.M. Moghaddas-Tafreshi, Bidding strategy of virtual power plant for participating in energy and spinning reserve markets—Part i: Problem formulation, IEEE Trans. Power Syst. 26 (2) (2010) 949–956.

[14] W. Zhong, M.A.A. Murad, M. Liu, F. Milano, Impact of virtual power plants on power system short-term transient response, Electr. Power Syst. Res. 189 (2020) 106609.

[15] C. Yuen, A. Oudalov, A. Timbus, The provision of frequency control reserves from multiple microgrids, IEEE Trans. Ind. Electron. 58 (1) (2010) 173–183.

[16] P. Ferraro, E. Crisostomi, M. Raugi, F. Milano, Analysis of the impact of microgrid penetration on power system dynamics, IEEE Trans. Power Syst. 32 (5) (2017) 4101–4109.

[17] A. Ouammi, H. Dagdougui, R. Sacile, Optimal control of power flows and energy local storages in a network of microgrids modeled as a system of systems, IEEE Trans. Control Syst. Technol. 23 (1) (2014) 128–138.

[18] J.S. Giraldo, J.A. Castrillon, C.A. Castro, F. Milano, Optimal energy management of unbalanced three-phase grid-connected microgrids, in: 2019 IEEE Milan PowerTech, 2019, pp. 1–6.

[19] D.A. Contreras, K. Rudion, Computing the feasible operating region of active distribution networks: Comparison and validation of random sampling and optimal power flow based methods, IET Gener., Trans. Distr. 15 (10) (2021) 1600–1612.

[20] Z. Chen, Z. Li, C. Guo, J. Wang, Y. Ding, Fully distributed robust reserve scheduling for coupled transmission and distribution systems, IEEE Trans. Power Syst. 36 (1) (2021) 169–182.

[21] J.S. Giraldo, J.C. López, J.A. Castrillon, M.J. Rider, C.A. Castro, Probabilistic OPF model for unbalanced three-phase electrical distribution systems considering robust constraints, IEEE Trans. Power Syst. 34 (5) (2019) 3443–3454.

[22] F. Milano, R. Zárate-Miñano, A systematic method to model power systems as stochastic differential algebraic equations, IEEE Trans. Power Syst. 28 (4) (2013) 4537–4544.

[23] F. Milano, Power System Modelling and Scripting, Springer, London, 2010.

[24] T. Kërçi, J. Giraldo, F. Milano, Analysis of the impact of sub-hourly unit commitment on power system dynamics, Int. J. Electr. Power Energy Syst. 119 (2020) 105819.

[25] Illinois Center for a Smarter Electric Grid, https://icseg.iti.illinois.edu/ieee-39-bus-system/.

[26] F. Milano, A python-based software tool for power system analysis, in: 2013 IEEE Power Energy Society General Meeting, 2013, pp. 1–5.

[27] W. Zhong, G. Tzounas, F. Milano, Improving the power system dynamic response through a combined voltage-frequency control of distributed energy resources, IEEE Trans. Power Syst. (2022) 1.